ISSN 1027-5495. Functional Materials, 33, No.3 (2026), p. 444-455
doi:http://dx.doi.org/10.15407/fm33.03.444 © 2026 — SSI "Institute for Single Crystals"
This is an open access article under the CC BY-NC-ND license (http://creativecommons.org/licenses/by-nc-nd/4.0/).

Fractal analysis of morphology of TBs-system and the effect of long-term aging on electrical transport in pure and aluminum-doped $YBa_2Cu_3O_{7-\delta}$ single crystals

O. Lazorenko[1], S. Vovk[2], R. Vovk[1]

[1]School of Physics, V. N. Karazin Kharkiv National University, 4, Svoboda Sq., 61022, Kharkiv, Ukraine
[2]Institute of Physics of the Czech Academy of Sciences, Na Slovance 1999/2, CZ-18221, Prague 8, Czech Republic.
Corresponding author e-mail:

Received May 10, 2026, approved July 05, 2026

The in-plane conductivity of pure and aluminum-doped $YBa_2Cu_3O_{7-\delta}$ single crystals was studied before and after long-term exposure in an air atmosphere. It was shown that prolonged exposure leads to an increase in the number of effective scattering centers for normal carriers. Aluminum doping partially slows down the degradation of conductive properties during the aging of experimental samples. The excess conductivity of the studied samples shows an exponential temperature dependence in a wide temperature range, and near T_c it is satisfactorily described by the Aslamazov–Larkin theoretical model. At the same time, long-term exposure significantly broadens the temperature range of the pseudogap state and substantially narrows the temperature interval of the linear dependence $\rho_{ab}(T)$. To investigate the peculiarities of the "tweed" structures, the fractal analysis method based on the box fractal dimension estimation was performed.

Keywords: fluctuation conductivity, fractal analysis, box fractal dimension, crossover, coherence length.

Фрактальний аналіз морфології TBs-системи та вплив тривалого старіння на електротранспорт у чистих та легованих алюмінієм монокристалах $YBa_2Cu_3O_{7-\delta}$.
О..Лазоренко, С.. Вовк, Р.. Вовк

Досліджено площинну провідність чистих та легованих алюмінієм монокристалів $YBa_2Cu_3O_{7-\delta}$ до та після тривалої експозиції в атмосфері повітря. Показано, що тривала експозиція призводить до збільшення кількості ефективних центрів розсіювання для нормальних носіїв заряду. Легування алюмінієм частково уповільнює деградацію провідних властивостей під час старіння експериментальних зразків. Надмірна провідність досліджуваних зразків у широкому діапазоні температур має експоненціальну температурну залежність, і поблизу T_c вона задовільно описується теоретичною моделлю Асламазова-Ларкіна. Водночас тривала експозиція значно розширює температурний діапазон псевдощілинного стану та суттєво звужує температурний інтервал лінійної залежності $\rho_{ab}(T)$. Для дослідження особливостей структур «твід» було застосовано метод фрактального аналізу, заснований на оцінці клітинної фрактальної розмірності.

1. Introduction

In recent years, there has been a clear trend toward expanding the scope of research dedicated to the potential technological applications of high-temperature superconductors (HTSCs) [1]. This is primarily due to the increasingly intensive use of these compounds in modern microelectronics, telecommunication systems, and so on. The $YBa_2Cu_3O_{7-\delta}$ compounds (the 1–2–3 system) are the most promising in this respect, for several reasons: these superconductors have a high critical temperature exceeding that of liquid nitrogen; their structure and conductive properties can be relatively easily tuned by changing the oxygen content [2] and substituting their components with isoelectronic analogues [3]. These compounds almost always contain twin boundaries (TBs), which significantly expands the scope of research [4].

All of the above-mentioned features raise a number of related questions and new problems. For example, the presence of labile oxygen in $YBa_2Cu_3O_{7-\delta}$ often leads to nonequilibrium states in the system, which can be induced by temperature [2, 3] or high pressure [4–6]. As a rule, such phenomena are observed in oxygen non-stoichiometric samples and practically do not appear in samples with a small oxygen deficiency $\delta \leq 0.15$ [7]. Several works [8–10] have reported possible changes in the superconducting and electrical transport properties during long-term exposure of 1–2–3 system samples in air. However, the experimental data obtained are often contradictory. For example, in [11] a significant improvement in electrical transport and an increase in critical current during long-term exposure to air were reported; whereas in [8–10], a significant deterioration in these properties was noted with long-term exposure to air. The substitution of $YBa_2Cu_3O_{7-\delta}$ components is also an important tool for finding empirical ways to improve their technological parameters. It is known that substituting yttrium with rare-earth elements (except praseodymium, which suppresses the superconducting parameters of the compound [12]) has little effect on their physical characteristics in the normal and superconducting states [3,4,13]. A significant role is played by the partial substitution of copper with elements such as gold, silver, and aluminum [14–18]. Gold and silver in small concentrations improve the conductivity of these compounds and hinder the degradation of their superconducting properties during aging [14,15].

Data on the effect of aluminum on the electrical transport properties of $YBa_2Cu_3O_{7-\delta}$ remain inconclusive. For example, in [16] a slight increase in in-plane resistivity ρ_{ab} was reported in $YBa_2Cu_{3-y}Al_yO_{7-\delta}$ crystals at $y \leq 10\%$, while in [17] a twofold increase in ρ_{ab} was observed at the same aluminum concentration. This discrepancy was probably due to the inhomogeneous distribution of aluminum in the crystal volume, since aluminum incorporation occurs uncontrollably during crystal growth in alumina crucibles. Evidence for such inhomogeneous distribution includes broad superconducting transitions $\Delta T_c \geq 2$K and their step-like form [16,17], as well as a significant scatter in superconducting parameters.

It should also be noted that aluminum doping reduces the period of the twinning superstructure by several times [18], and at higher concentrations leads to the formation of a structure of intersecting "tweed"-type twin domains [19]. TBs, being extended planar defects, enhance pinning processes [20], thereby expanding the area of possible applications for generating high magnetic fields. At the same time, the presence of TBs often complicates the study of resistive characteristics due to difficulties in determining their contribution to the conductivity of HTSC compounds [18].

The effect of aluminum doping on aging processes also remains an open question. Taking into account all of the above, this paper investigates the effect of long-term exposure to an air atmosphere on various conductivity modes of pure and aluminum-doped $YBa_2Cu_3O_{7-\delta}$ single crystals with high critical temperature T_c and a system of unidirectional twin planes, provided that the transport current vector $I \| \perp$TB, where the influence of twins on the scattering processes of charge carriers is minimal. Considering that long-term exposure affects the homogeneity of samples, an attempt was made to describe their properties using fractal analysis.

2. Experimental methodology

The $YBa_2Cu_3O_{7-\delta}$ single crystals were grown in a gold crucible by melting from a solution with a small temperature gradient along the crucible [18]. The source materials were Y_2O_3, $BaCO_3$, and CuO powders. To obtain aluminum doped single crystals, 0.2 wt.% Al_2O_3 was added. For the resistivity measurements, the following single crystals were selected: K1– ($YBa_2Cu_3O_{7-\delta}$) with dimensions 2×0.3×0.02 mm^3, and crystal K2– ($YBa_2Cu_{3-y}Al_yO_{7-\delta}$) with dimensions

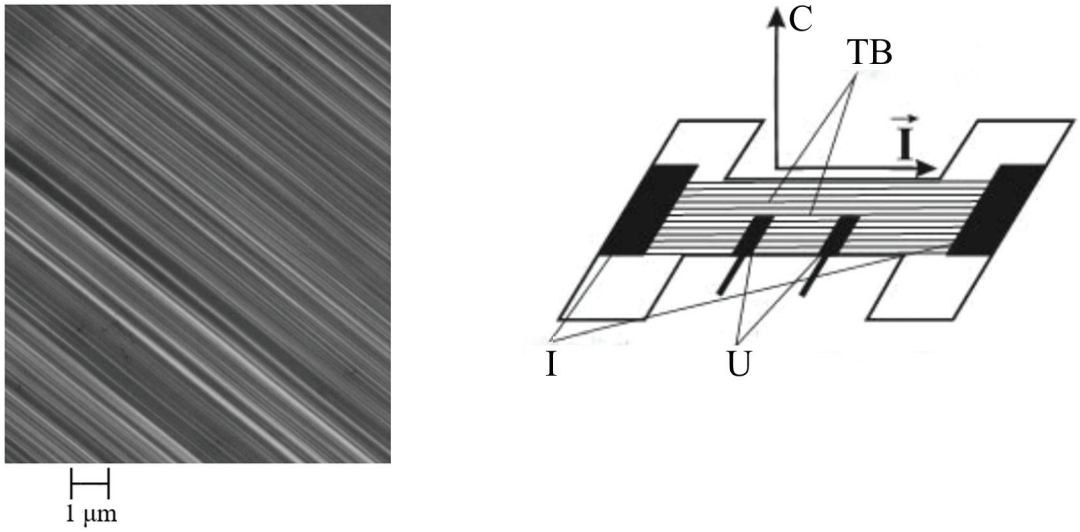

Fig. 1. Photograph of a region with unidirectional twin boundaries in the K2 crystal (left), and the geometry of the experiment (right)

2.3×0.75×0.03 mm^3. In all the samples the ***c***-axis was oriented along the smallest dimension. Both single crystals had areas with unidirectional twin boundaries measuring 0.5×0.5 mm^2 (Fig. 1). This geometric shape was chosen so that we could cut bridges with parallel TBs of 0.2 mm width at distance of 0.3 mm between pairs of contacts (see Fig. 1). The standard four-contact scheme was used. Silver paste was applied to the crystal surface and the junction of gold wires (0.05 mm in diameter), followed by a three-day annealing at 420 °C in an oxygen atmosphere to achieve an optimal oxygen concentration and a high point T_c. The technique provided a contact resistance of less than 1 Ohm and made it possible to measure the resistivity at transport currents of up to 10 mA in the ***ab***-plane. The temperature was measured with a copper-constantan thermocouple. The first measurements of the electrical resistivity in the basal ***ab***-plane were performed immediately after removing the crystal from the melt and their oxygen saturation to the optimum value ($\delta \leq 0.1$). After these measurements, the crystal was stored in a glass container until the re-measurements, which were carried out after 6 years.

Fig. 1 shows a photograph of the surface of an Al-doped crystal with a characteristic twin network pattern. As is well known, impurities of trivalent ions act as centers of defect formation [18, 19], and with an increase in their density, the period of the twin domain structure decreases. As a consequence, closely spaced microtwins may overlap, resulting in a tweed-like structure [19]. As can be seen from the figure, no tweed-like structure was observed in the studied $YBa_2Cu_{3-y}Al_yO_{7-\delta}$, crystals, which is likely due to the low concentration of Al, while the inter-twin spacing was two to three times smaller than in pure crystals.

2. Results and discussion

2.1 Resistivity

The temperature dependences of the in-plane resistivity, $\rho_{ab}(T)$, for crystals K1 and K2, measured before and after long-term exposure in an air atmosphere, are shown in Fig. 2(*a*) and 2(*b*), respectively. Resistive superconducting transitions of the same samples, plotted in the coordinates $\rho_{ab} - T$ and $d\rho_{ab}/dT - T$, are shown in the corresponding insets. It is evident that in all cases the dependences are quasi-metallic; however, the ratio ρ_{ab}(300 K)/ρ_{ab}(0 K), determined before and after prolonged air exposure, decreased significantly for crystals K1 and K2 – from 64 to 39 and from 12 to 8, respectively (the value of ρ_{ab}(0 K) was determined by interpolation of the linear temperature region of $\rho_{ab}(T)$, as shown in Fig. 2). At the same time, the ***ab***-plane resistivity at room temperature increased from 151 to 196 and from 421 to 453 μΩ·cm for K1 and K2, respectively, while their critical temperatures decreased from 92.01 to 90.83 K and from 92.05 to 90.85 K, respectively.

The width of the resistive superconducting transition ΔT_c increased significantly for both samples (from 0.3 and 0.5 K to ≈1 K for K1 and K2, respectively), and in the case of crystal K2, the transition acquired a stepwise shape. The

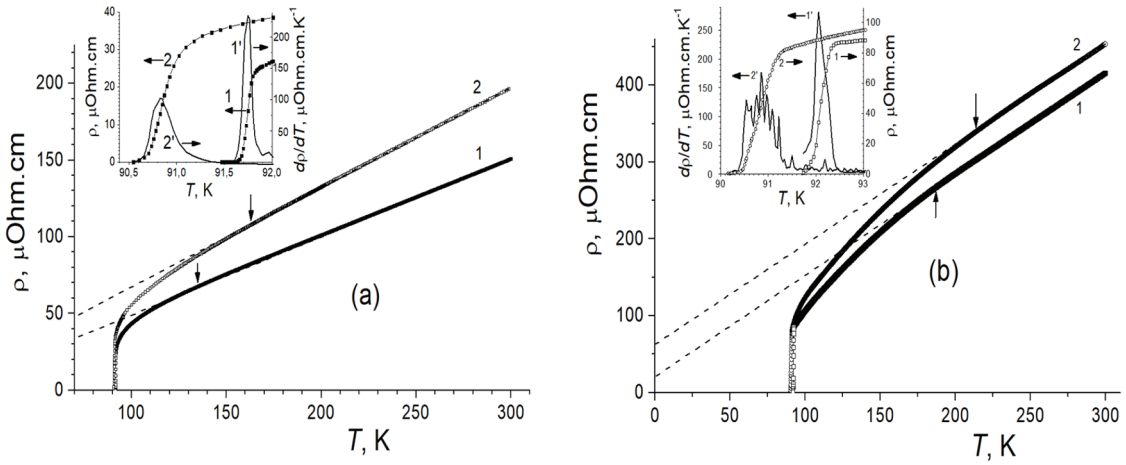

Fig. 2. The $\rho_{ab}(T)$ dependence of the $YBa_2Cu_3O_{7-\delta}$ (a) and $YBa_2Cu_{3-y}Al_yO_{7-\delta}$ (b) single crystals, before and after long-term exposure to air, curves 1 and 2, respectively. The arrows show the pseudogap opening temperature, T^*. The insets show the transitions to the superconducting state in $\rho_{ab} - T$ and $d\rho_{ab}/dT - T$ coordinates for the same samples. The numbering of the curves in the insets corresponds to the numbering in the figure

parameters of the studied samples are presented in Table 1. Using literature data on the dependence of T_c on oxygen concentration [21], it can be concluded that the oxygen content decreased slightly (by 1–2%) during exposure in both crystals and remained within $\delta \leq 0.15$ [21].

The increase in the width of the resistive transitions in crystals K1 and K2 indicates a reduction in the degree of homogeneity of the studied samples [3,4,6,7], while the stepped shape observed after exposure of crystal K2 points to the appearance of signs of phase separation within their volume [4,6]. The latter assumption is supported by the presence of a number of small peaks in the $d\rho_{ab}/dT - T$ dependence of crystal K2. According to [3], these peaks correspond to the T_c of different phases inside the crystal. The absence of such peaks in the case of crystal K1 suggests the possible existence of percolative current pathways through the phase with the higher T_c [22].

As follows from the obtained results, the relative change in resistive parameters during aging was significantly larger in the undoped crystal K1 than in the Al-doped crystal K2. Since in all samples the current vector $\boldsymbol{I}$ was oriented parallel to the TBs, this difference could not be caused by the higher TBs density in the Al-doped crystal, which has a smaller intertwin spacing. The observed increase in ρ_{ab} during aging is likely due to a decrease in the carrier density or the appearance of effective scattering centers, as also indicated by the change in the ratio $\rho_{ab}(300\ \text{K})/\rho_{ab}(0\ \text{K})$. The increase in the number of vacancies formed during prolonged exposure of samples to air increases the degree of non-stoichiometry of the compound, probably as a result of partial loss of oxygen; the vacancies can serve as scattering centers. At the same time, as noted above, in crystal K2 several peaks appeared in the $d\rho_{ab}(T)/dT$ dependence may indicate an increase in the number of different phase inclusions [22] inside the sample. As is known [18], aluminum impurities with trivalent ions, having a significantly smaller ionic radius compared to copper, act as centers of defect formation. Aluminum atoms may form a characteristic octahedral coordination with oxygen atoms [18], which in turn may promote the decomposition of the conducting subsystem into several phases with different T_c values. The presence of such phases can manifest itself in the form of steps in resistive superconducting transitions (and corresponding peaks in the $d\rho_{ab}/dT - T$ coordinates) [3,4,6,7], and also change the mechanism of diffusion processes, thereby probably reducing the intensity of deoxygenation of the experimental sample volume.

Thus, doping with aluminum leads to an increase in the heterogeneity of the sample of the 1-2-3 system, associated not only with the system of defects, but also with the electronic structure.

2.2 Fluctuation conductivity

As can be seen from Fig. 2, when the temperature decreases below a certain characteristic value T^*, the $\rho_{ab}(T)$ dependence deviates from linearity, which indicates the emergence

Table 1. Resistivity parameters before and after aging of the samples

Samples		T_c, K	ρ_{ab}(300 K), μΩ·cm	T*, K	Δ^*_{ab}, meV	ε_0	α_{3D}	α_{2D}	$\xi_c(0)$, Å
K1	Before aging	92.01	151	138	88.7	0.061	-0.508	-1.084	1.45
	After aging	90.83	196	167	66.3	0.088	-0.503	-1.062	1.74
K2	Before aging	92.05	421	199	58.1	0.157	-0.506	-0.990	2.32
	After aging	90.85	453	228	45.5	0.188	-0.495	-1.017	2.54

of excess conductivity. According to current understanding, this is caused by the onset of the pseudogap (PG) regime [23–25]. At present, two main scenarios for the appearance of the PG anomaly in HTSC systems are widely debated in the literature. According to the first, the appearance of the PG is associated with short-range "dielectric"-type fluctuations, which occur in underdoped compositions (see e.g., the review [23]). The second scenario assumes the formation of Cooper pairs already at temperatures well above the critical temperature ($T^* >> T_c$), with their subsequent establishment of phase coherence only at $T < T_c$ [24,25].

As can be seen from Table 1 and Fig. 2, long-term annealing leads to a significant narrowing of the region of linear dependence $\rho_{ab}(T)$ in both crystals compared with the initial samples, while the temperature T^* shifts toward higher temperatures by 29 K for both single crystals K1 and K2. This indicates a corresponding expansion of the temperature interval of excess conductivity.

The temperature dependence of the excess conductivity is usually determined from the equality:

$$\Delta\sigma = \sigma - \sigma_0, \quad (1)$$

where $\sigma_0=\rho_0^{-1}=(A+BT)^{-1}$ is the conductivity determined by extrapolating the linear region to zero temperature, and $\sigma=\rho^{-1}$ is the experimentally measured conductivity in the normal state. The obtained experimental dependences $\Delta\sigma(T)$ are presented in Fig. 3 in $\ln\Delta\sigma - 1/T$ coordinates. It can be seen that, within a fairly wide temperature interval, these dependences are straight lines, which corresponds to their description by an exponential dependence of the form:

$$\Delta\sigma \sim \exp(\Delta^*_{ab}/T), \quad (2)$$

where Δ^*_{ab} characterizes a certain thermally activated process through a pseudogap.

An exponential dependence of $\Delta\sigma(T)$ has already been observed earlier in YBaCuO samples [24]. At the same time, the approximation of experimental data can be significantly improved by introducing a multiplier $(1–T/T^*)$. In this case, the excess conductivity turns out to be proportional to the density of superconducting carriers $n_s \sim (1–T/T^*)$ and inversely proportional to the number of pairs $\sim \exp(–\Delta^*/kT)$ destroyed by thermal motion. Here T^* is considered as the mean-field temperature of the superconducting transition, and the temperature interval $T_c<T<T^*$, within which the PG state exists, is determined by the stiffness of the order parameter phase, which in turn depends on the oxygen deficiency or the concentration of the dopant element. Some role may also be played by the influence of other specific mechanisms of quasiparticle interaction [26], caused by the presence of structural and kinematic anisotropy in the system. The value of Δ^* obtained from (2) for our experimental samples is given in Table 1. It can be seen that long-term annealing leads to a significant decrease in the absolute value of the pseudogap: $\Delta^*_1/\Delta^*_2 \approx 1.34$ and $\Delta^*_1/\Delta^*_2 \approx 1.28$ for crystals K1 and K2, respectively.

Fig. 3 shows that as T_c is approached, $\Delta\sigma$ increases sharply. According to theory [27], in the vicinity of T_c the excess conductivity is due to fluctuation pairing of carriers, whose contribution to conductivity for $T > T_c$ in the two-dimensional (2D) and three-dimensional (3D) cases is determined by power-law dependences of the form:

$$\Delta\sigma_{2D} = \frac{e^2}{16\hbar d}\varepsilon^{-1}, \quad (3)$$

$$\Delta\sigma_{3D} = \frac{e^2}{32\hbar\xi_c(0)}\varepsilon^{-1/2}, \quad (4)$$

where $\varepsilon = (T–T_c)/T_c$; e is the electron charge; $\xi_c(0)$ is the coherence length along the $\boldsymbol{c}$-axis at $T\to0$; and d is the characteristic thickness of the 2D layer. In our case, T_c was determined at the maximum point of the $d\rho_{ab}(T)/dT$ dependences in the region of the superconducting transition (insets to Fig. 2).

The insets to Fig. 3 show the temperature dependences $\Delta\sigma(T)$ in $\ln\Delta\sigma - \ln\varepsilon$ coordinates. It can be seen that, near T_c, these dependences are satisfactorily approximated by straight

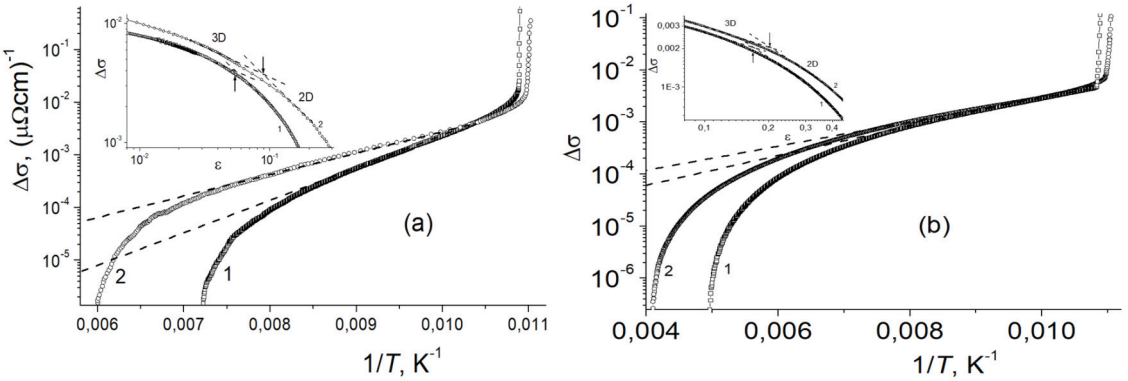

Fig. 3. Temperature dependence of excess conductivity in the ***ab***-plane of a $YBa_2Cu_3O_{7-\delta}$ single crystal in $\ln\Delta\sigma - 1/T$ and $\ln\Delta\sigma - \ln\varepsilon$ (inserts) coordinates. The designations of the curves in the main panel and in the insets are the same. In the main panel, the dotted lines show approximations by equation (2). In the insets: linear approximations with a slope of $tg\alpha_1 \approx -0.5$ (3D mode) and $tg\alpha_2 \approx -1.0$ (2D mode). Arrows indicate the 2D-3D intersection point.

lines with a slope of $tg\alpha_1 \approx -0.5$, corresponding to the power exponent –1/2 in equation (4), which clearly indicates the three-dimensional nature of fluctuation superconductivity in this temperature interval. With a further increase in temperature, the rate of decrease of $\Delta\sigma$ rises significantly ($tg\alpha_2 \approx -1$), which in turn can be regarded as evidence for a change in the dimensionality of fluctuation conductivity. As follows from (3) and (4), at the 2D–3D crossover point:

$$\xi_c(0)\varepsilon_0^{-1/2} = d/2. \qquad (5)$$

In this case, by determining the value of ε_0 and using literature data on the dependence of interplanar distance on δ [18,27] ($d \approx 11.7$ Å), one can calculate the values of $\xi_c(0)$. The performed calculations showed that, during aging, the coherence length changes from $\xi_c(0)$=1.45Å to $\xi_c(0)$=1.74Å for crystal K1, and from $\xi_c(0)$= 2.32 Å to $\xi_c(0)$= 2.54 Å for crystal K2. At the same time, the 3D–2D crossover point shifts significantly in temperature (see Table 1 and Fig. 3).

2.3. Fractal Analysis

Since $YBa_2Cu_3O_{7-\delta}$ single crystals represent a very complex, open, non-linear quantum-mechanical system, the so-called nonlinear and system paradigms [28] proposed 1980s by Prof. L. Chernogor (Kharkiv, Ukraine) can be successfully applied to describe their properties. According to these paradigms, such systems, in particular, can potentially possess fractal properties in one form or another. Moreover, the fractal paradigm [29, 30] formulated in 2003 by Prof. V. Yanovsky (Kharkiv, Ukraine) states that fractality is apparently one of the fundamental properties of the surrounding world as a whole. Thus, it is interesting to search for such properties in the $YBa_2Cu_3O_{7-\delta}$ system. We believe that this approach was successfully applied in the present study.

Today it is well known that as a fundamentally new approach in modern science and engineering, the fractal concept was proposed in 1975 by world famous American mathematician and physicist B. Mandelbrot [31 – 34]. From 1975 to present moment, this concept had been improved and transformed from a dubious, strange and unclear theory to one of the most modern, well-grounded and quite solid approaches proposed by the human civilization (see, for example, [34 – 40]). A short review of the fractal approach evolution can be found, for example, in the paper [41].

It is important to point out that, as we know, the application of the concept of fractals is not at all a new idea for solid state physics in general (see, for example, [34, 35]) and for low temperature physics in particular (see, for example, [42 – 44]), but the way proposed in this paper seems to be quite original.

It seems somewhat surprising that, although at present day there is a set of different definitions of a fractal [41], there is no one strong and universal one. Nevertheless, the most successful and generally accepted definition was formulated by famous American researcher K. Falconer in 1990 and some of its improvements and additions were made by him in 1996 [45]. According to this, a set R is called a fractal, if its properties include the following: 1) the set R has a fine structure, i.e. it is detailed at the smallest scales; 2) the set R is a sufficiently irregular structure that it could be described by traditional geometric methods

(Euclidean or Lobachevsky geometry, etc.) both at the local level and at the level of the entire structure; 3) the set R has a property of self-similarity both in an approximate form and in a statistical one; 4) usually the fractal dimension of a set R (defined in some way) turns out to be greater than its topological dimension; 5) in most cases the set R is defined in a very simple way, possibly recursively; 6) often the set R is of natural origin. All fractals are divided into mathematical and physical, or natural, ones. Firsts of them are pure theoretical objects existing in the imagination of the mathematicians only, but the seconds of them are surely appeared to be the real existing objects from surrounding world. Namely, the properties of a physical fractal should be searched for the $YBa_2Cu_3O_{7-\delta}$ system.

To describe these, the numerical characteristics of The fractal are usually used. The most frequently applied characteristics is a fractal dimension (see, for example, [33, 46]). Unlike the Euclidean D_E dimension of the space in which an object was immersed and the topological D_T of an object itself, a fractal dimension D_F, as a rule, should satisfy the relation $D_E \geq D_F > D_T$ and can usually be fractional, but its integer values are not prohibited too (for example, it is so for the so-called Peano curves). The physical sense of a fractal dimension is how densely a fractal fills the Euclidean space: the bigger a fractal dimension value appears, the more densely the space was filled. For correct comparisons of the fractal dimensions of the structures discussed below, it is important to note, that if the fractal dimensions of two different objects turn out to be equal, this does not necessarily mean that there is any similarity in their structure.

In our investigations of the fractal properties of the $YBa_2Cu_3O_{7-\delta}$ system, the experimental images similar to those shown in Fig. 1 were chosen as objects of study. On the one hand, from the point of view of mathematical analysis, each such image in shades of gray (8 bit) is a $M \times N$ matrix containing a set of the real discrete counts of the real-valued function $z = f(x,y)$, obtained in the (x_i, y_j) points, where $i = 1, M$ and $j = 1, N$. On the other hand, set theory states that this image can be viewed as a set of points with given coordinates (x_i, y_j, z_{ij}) located in ordinary 3d space. For this set, a fractal dimension D_F can be estimated in some way (see, for example [47]). As is usual for discrete images, it is convenient to use all geometric dimensions of the objects under study, represented in pixels.

Apart from the fact that there are many different fractal dimensions used for the physical fractals and methods for their calculation, the problem of choosing the appropriate fractal dimension for a particular case seems to be a question that is completely beyond the scope of this paper [48]. In this paper, we chosider only one of them, namely, the oldest one called the box dimension D_B. Typically, its estimation is performed using the so-called box-counting method, which is based on iteratively covering a set located in the d^n space with generalized spheres (or boxes) with gradually decreasing size $r(k)$ and calculating the required number $N(k)$ of such spheres. For a mathematical fractal, if the number of the iterative process steps tends to infinity ($k \to \infty$), the box dimension D_B can be estimated as

$$D_B = \lim_{k \to \infty} \frac{\log N(k)}{\log \frac{1}{r(k)}}. \qquad (6)$$

However, for a physical fractal, where the value of k is always limited, and the minimum value of $r(k)$ is in principle greater than zero, this approach seems completely unacceptable; thus, some other method must be used. This option exists and is based on the fact that for a physical fractal the relationship between $\log N(k)$ and $\log r(k)$ must be linear. Then, by approximating the existing experimental points on the plane $(\log N(k), \log r(k))$ with a straight line using the least squares method, the value of the box dimension D_B can be successfully obtained from the slope of this line. In addition, the error in estimating the box dimension ΔD_B has also become available for evaluation.

The results of this approach realized for three different experimental images are presented in Fig. 4. First of them (Fig. 4(a)) is the K2 ($YBa_2Cu_{3-y}Al_yO_{7-\delta}$) crystal (the image sizes are 3210×2707 pixels). In the sense described above, it has some fractal properties for $-7 \leq \log r \leq -1$, namely, its box fractal dimension is $D_B = 2.46 \pm 0.02$ for $L = 0.1 \div 6.1$ μm, where L is the size range (in μm) in which the fractal properties of the K2 crystal exist. It is important to note that in Fig. 4(d) the least squares fitting line (dashed line) is only plotted over a limited range ($-7 \leq \log r \leq -1$).

However, over the entire available range ($-11 \leq \log r \leq -1$), the crystal K2 image turned out to be non-fractal, and also the existing experimental points are not located on the same

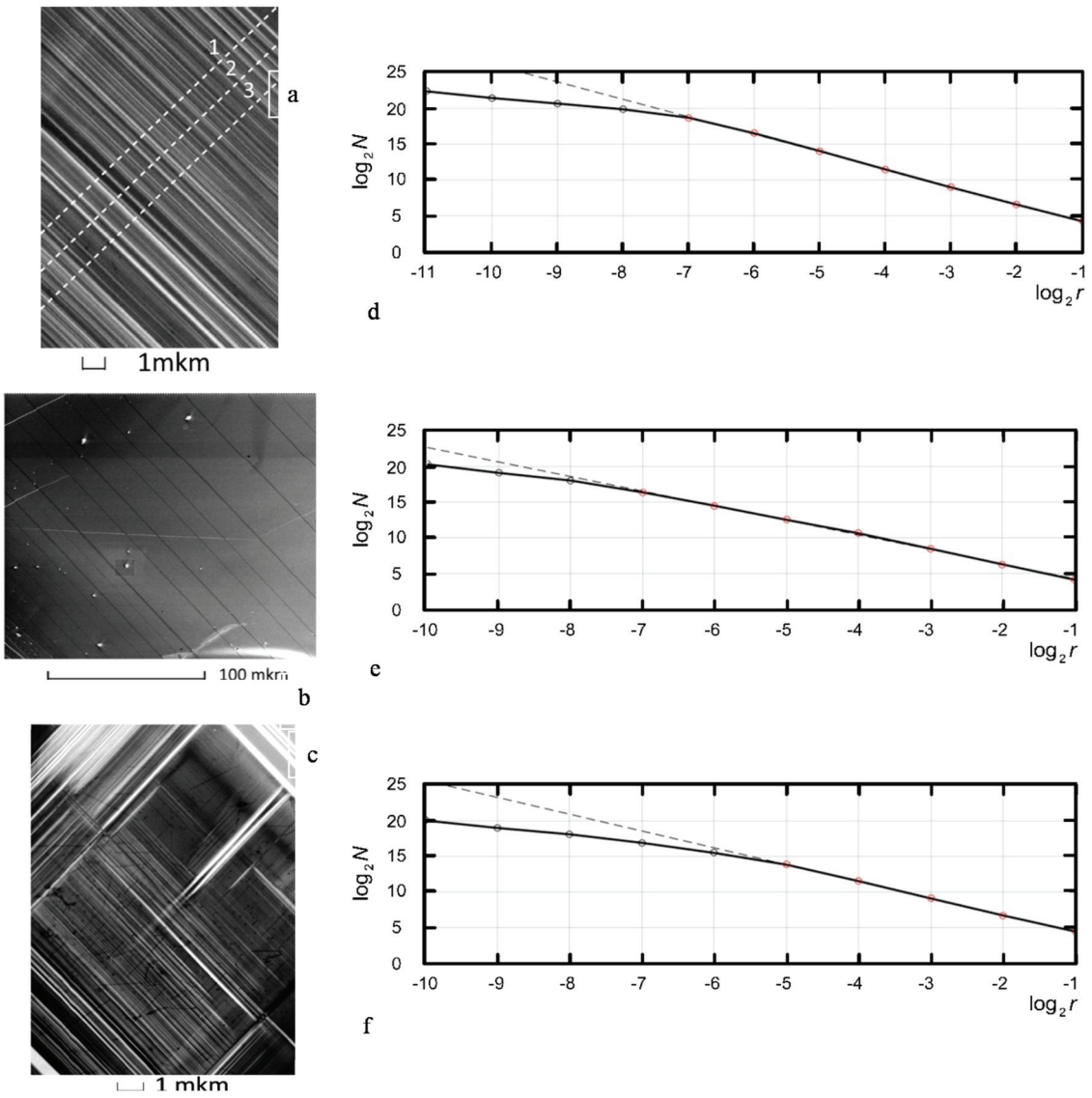

Fig. 4. The $\log N$ vs $\log r$ dependences (d, e, f) for the K2 ($YBa_2Cu_{3-y}Al_yO_{7-\delta}$) crystal (a), the $YBa_2Cu_3O_{7-\delta}$ crystals with 'twinned' structures occurred during the cultivation process (b) and after annealing in an oxygen atmosphere (c), respectively. The dashed lines show the approximating straight lines constructed using the least squares method for $-7 \le \log r \le -1$ (d, e) and for $-5 \le \log r \le -1$ (f). In image (a),

straight line. The second image (Fig., 4b) shows an $YBa_2Cu_3O_{7-\delta}$ crystal with a "twinned" structure formed during the cultivation process. This image, obtained using an optical microscope has the sizes equal to 1341×1626 pixels. It appears to have some fractal properties (Fig. 4, e) for $-7 \le \log r \le -1$; the fractal dimension of its box is apparently equal to $D_B = 2.05 \pm 0.04$ for $L = 1.6 \div 99.5$ μm. The third image (Fig. 4, c) obtained with an electron microscope corresponds to a $YBa_2Cu_3O_{7-\delta}$ crystal with "twinned" structure occurred after annealing in an oxygen atmosphere. It has the sizes equal to 1341×1626 pixels. The fractal properties of this structure exist for $-5 \le \log r \le -1$ (Fig. 4, f), its box fractal dimension $D_B = 2.38 \pm 0.01$ for $L = 0.5 \div 8.1$ μm.

To search for additional fractal properties of the first image (Fig. 4, a), the original idea implemented below seems interesting, useful and relevant. In addition to the characteristic striped structure of this image (Fig. 4, a), the $z = f(x, y)$ the surface can be successfully intersected by planes located perpendicular to both the image plane and these stripes. As a result, the cross-section is represented as a one-dimensional signal, which may also be fractal.

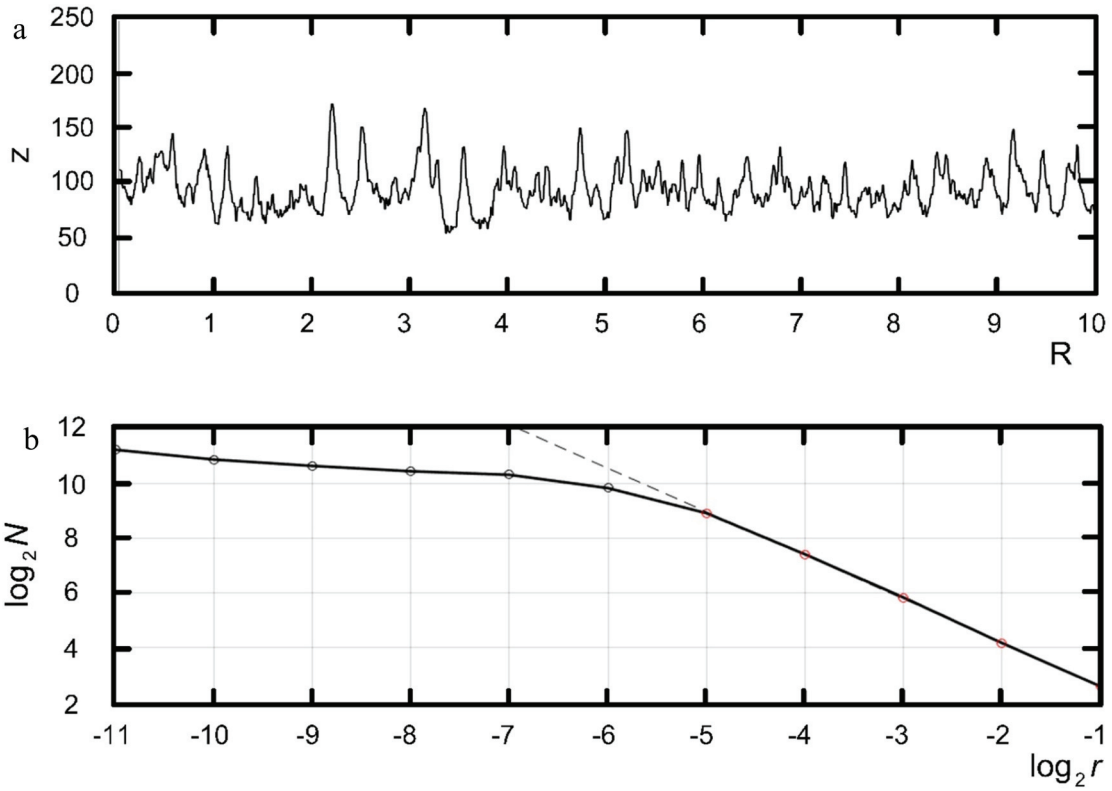

Fig. 5. Dependence $\log N$ vs $\log r$ (b) for the $YBa_2Cu_3O_{7-\delta}$ crystals with 'twin' structures formed during cultivation (b). The dashed line shows the approximating straight line constructed with the least square method for $-5 \le \log r \le -1$. Subplot (a) shows the one-dimensional signal $z = f(R)$ obtained as a result by intersecting the surface $z = f(x, y)$ with plane '2' located perpendicular to both the image plane and the stripes in Fig. 4, a. Here R is a dimensionless spatial variable

In our calculations, three such planes named as '1', 2' and '3' (Fig. 4(a)) were constructed.

Although all three signals containing 2707 points turned out to be very similar, the analysis results in Fig. 5 are shown only for one of them, namely for signal "2". It was found that fractal properties of all signals exist for $-5 \le \log r \le -1$ ($L = 0.5 \div 7.2$ μm); their fractal dimensions of the box turned out to be $D_B = 1.57 \pm 0.01$ for the signal '1', $D_B = 1.59 \pm 0.01$ for the signal '2' and $D_B = 1.57 \pm 0.02$ for the signal '3'.

The results obtained using fractal analysis and described above allow us to draw a number of important and valuable conclusions.

Firstly, 'twin' structures observed in K2 ($YBa_2Cu_{3-y}Al_yO_{7-\delta}$) and $YBa_2Cu_3O_{7-\delta}$ crystals were found to exhibit pronounced fractality.

Secondly, as is always observed in the case of physical (natural) fractals, fractal properties exist in a limited range of spatial dimensions, and not in all existing ones. As our experimental data showed, this range is approximately $L \sim 0.1 \div 10$ μm. For this reason, the use of an electron microscope seems preferable for studying the fractal properties of crystals with a "twin" structure. At this point we are not confirming this, we are only assuming. However, it is precisely this assumption that can successfully explain the results obtained for the $YBa_2Cu_3O_{7-\delta}$ crystal with "twin" structures formed during the cultivation process (Fig. 4,b, e). Even when simply viewed without any pre-processing, it is clear that the image (Fig. 4(b)) looks very smooth, without any significant damage or cracks. Since the box fractal dimension value ($D_B = 2.05 \pm 0.04$ for $L = 1.6 \div 99.5$ μm) obtained above for this case is practically no different from the value for a non-fractal image (theoretically $D_B = 2.00$), the image (Fig. 4,b) can be classified as non-fractal. But what is the real reason for this? Most likely, the problem lies in the relatively low resolution of the optical microscope that created this image.

Thirdly, the significant downward deviations of experimental data points from the approximating straight lines observed in Fig. 4(d – f) and Fig. 5, b can be explained both by the real fractal properties of the physical structure under study and by the "depletion"

phenomenon, well known to specialists since the 1980s (see, for example, [33, 36, 46, 47]). The latter factor turned out to be very significant, especially in relation to the box dimension D_B, when the covering box size turns out to be too small, and, therefore, the number of the boxes turns out to be too large, while the number of real fractal points remains very limited. In our opinion, the second reason seems the most likely. To successfully solve this problem, it is necessary to increase the number of points in the image and improve the spatial resolution of the experimental equipment.

Fourth, if a crystal with a "twinned" structure is characterized by pure striped structure (see, for example, Fig. 4, a), and not cross-striped structure (see, for example, Fig. 4, c), then in the case of a crystal with a "twinned" structure, all one-dimensional signals arising from the intersection of the surface $z = f(x, y)$ with planes perpendicular to both the stripes and the image plane turn out to be very similar and fractal. The spatial range of their fractality is approximately the same as that of the corresponding image ($L \sim 0.1 \div 10\,\mu m$). As a result, the values of the box dimension D_B for all such planes turn out to be practically the same.

4. Conclusions

In conclusion, we briefly summarize the main results obtained in this work.

1. Long-term exposure of oxygen-optimally doped YBaCuO single crystals in air leads to partial deterioration of conductive properties and the appearance of effective scattering centers for charge carriers. The introduction of aluminum impurities partially helps to slow down the deterioration of conductive properties during the aging process of experimental samples. The excess conductivity $\Delta\sigma(T)$ of pure and Al-doped YBaCuO single crystals, in a wide temperature range $T_c<T<T^*$, follows an exponential temperature dependence and, in the vicinity of T_c, is satisfactorily described within the framework of the Aslamazov–Larkin theoretical model. At the same time, prolonged exposure to air significantly broadens the temperature interval of the pseudogap state in the *ab*-plane, thereby narrowing the linear region of $\rho_{ab}(T)$. During aging, signs of phase separation also appear in the volume of the experimental samples, manifested in the form of additional peaks in the $d\rho_{ab}(T)/dT$ dependences in the region of the superconducting transition.

2. The 'twin' structure observed in crystals, in particular, in the K2 ($YBa_2Cu_{3-y}Al_yO_{7-\delta}$) crystal and the $YBa_2Cu_3O_{7-\delta}$ crystal, was found to be generally quite fractal over a limited range of spatial dimensions, although not for all existing ones. Nevertheless, this fact allows us to begin the process of studying the fractal and multifractal properties of crystals with a "twin" structure and other similar structures. Modern methods of fractal and multifractal analysis, being powerful tools for digital analysis of signals and images, allow us to obtain a set of various numerical characteristics that describe in sufficient detail the fractal and multifractal properties of the object under study. In future studies planned by the authors, they hope to discover and study unknown relationships between these numerical characteristics and characteristics describing the "traditional" physical properties of the structures under study.

Acknowledgment:

S.V. are grateful for the support of the Ministry of Education, Youth and Sports of the Czech Republic within the framework of the project "Multifunctionality of Ferroids" [Project № CZ.02.01.01/00/22008/0004591].

References

1. C. V. Varanasi, J. Burke, H. Wang, J. H. Lee and P. N. Barnes, 2008. Thick $YBa_2Cu_3O_{7-x}$ + $BaSnO_3$ films with enhanced critical current density at high magnetic fields. Appl. Phys. Lett. 93, 092501. https://doi.org/10.1063/1.2976683.
2. J. D. Jorgencen, Pei Shiyou, P. Lightfoot, H. Shi, A. P. Paulikas, B. M. W. Veal, Time-dependent structural phenomena at room temperature in quenched $YBa_2Cu3O_{6.41}$: Local oxygen ordering and superconductivity, Physica C. 167 (1990), 571 – 578. https://doi.org/10.1016/0921-4534(90)90676-6.
3. R. V. Vovk, M. A. Obolenskii, A. A. Zavgorodniy, I. L. Goulatis, V. I. Beletskii, A. Chroneos, Structural relaxation, metal- toinsulator transition and pseudo-gap in oxygen deficient $HoBa_2Cu_3O_{7-\delta}$, Physica C. 469 (2009), 203 – 206. https://doi.org/10.1016/j.physc.2009.01.011.
4. R. V. Vovk, Z. F. Nazyrov, M. A. Obolenskii, I. L. Goulatis, A. Chroneos, V. M. Pinto Simoes, Phase separation in oxygen deficient $HoBa_2Cu_3O_{7-\delta}$ single crystals: effect of high pressure and twin boundaries, Philosophical Magazine. 91 (2011), 2291 – 2302. https://doi.org/10.1080/14786435.2011.552893.

5. S. Sadewasser, J. S. Schilling, A. P. Paulicas, B. M. Veal, Pressure dependence of T_c to 17 GPa with and without relaxation effects in superconducting $Y_1Ba_2Cu_3O_x$, Phys. Rev. B. 61(1) (2000), 741 – 749. https://doi.org/10.1103/PhysRevB.61.741.
6. R. V. Vovk, G. Ya. Khadzhai, Z. F. Nazyrov, I. L. Goulatis, A. Chroneos, Relaxation of the normal electrical resistivity induced by high-pressure in strongly underdoped $YBa_2Cu_3O_{7-\delta}$ single crystals, Physica B. 407 (2012), 4470 – 4472. https://doi.org/10.1016/j.physb.2012.07.049.
7. R. V. Vovk, N. R. Vovk, G. Ya. Khadzhai, I. L. Goulatis, A. Chroneos, Effect of high pressure on the electrical resistivity of optimally doped $YBa_2Cu_3O_{7-\delta}$ single crystals with unidirectional planar defects, Physica B: Condensed Matter. 422 (2013), 33 – 35. http://dx.doi.org/10.1016/j.physb.2013.04.032.
8. Z. Li, H. Wang, N. Yang, X. Jin, L. Shen, J. Chin. Ceram. Soc. 18 (1990), 555-560.
9. K. Schlesier, H. Huhtinen, S. Granroth and P. Paturi, 2010. An aging effect and its origin in GdBCO thin films, J. Phys.: Conf. Ser. 234, 012036. https://doi.org/10.1088/1742-6596/234/1/012036.
10. B. Martínez, F. Sandiumenge, S. Piñol, N. Vilalta, J. Fontcuberta, X. Obradors, Aging of critical currents and irreversibility line in melt textured $YBa_2Cu_3O_7$, Applied Physics Letters. 66 (1995) 772 – 774. https://doi.org/10.1063/1.114089.
11. Qing-Rong Feng, Xing Zhu, Sun-Qi Feng, Han Zhang and Zi-Zhao Gan, Effect of time aging on the properties of Ag-doped YBaCuO superconductors, Supercond. Sci. Technol. 6 (1993), 715 – 720. https://doi.org/10.1088/0953-2048/6/10/002.
12. R. V. Vovk, Z. F. Nazyrov, I. L. Goulatis, A. Chroneos, Metal-to-insulator transition in $Y_{1-x}Pr_xBa_2Cu_3O_{7-\delta}$ single crystals with various praseodymium content, Physica C. 485 (2013), 89 – 91. http://dx.doi.org/10.1016/j.physc.2012.09.017.
13. R. V. Vovk, M. A. Obolenskii, A. V. Bondarenko, I. L. Goulatis, A. V. Samoilov, A. I. Chroneos, V. M. Pinto Simoes, Transport anisotropy and pseudo-gap state in oxygen deficient $ReBa_2Cu_3O_{7-\delta}$ (Re = Y, Ho) single crystals, J. Alloys and Compounds, 464 (2008), 58 – 66. https://doi.org/10.1016/j.jallcom.2007.10.040.
14. M. Z. Cieplak, Gang Xiao, C. L. Chien, A. Bakhshai, D. Artymowicz, W. Bryden, J. K. Stalick and J. J. Rhyne, Incorporation of gold into $YBa_2Cu_3O_7$: Structure and *Tc* enhancement, Phys. Rev. B. 42 (1990), 6200 – 6208. https://doi.org/10.1103/PhysRevB.42.6200.
15. D. A. Lotnyk, R. V. Vovk, M. A. Obolenskii, A. A. Zavgorodniy, J. Kováč, M. Kaňuchová, M. Šefciková, V. Antal, P. Diko, A. Feher, A. Chroneos, Evolution of the Fishtail-Effect in Pure and Ag-doped MG-YBCO, Journal of Low Temperature Physics. 161 (2010), 387 – 394. https://doi.org/10.1007/s10909-010-0198-z.
16. R. B. van Dover, L. F. Schneemeyer, J. V. Waszczak, D. A. Rudman and J. Y. Juang, J. A. Cutro, Extraordinary effect of aluminum substitution on the upper critical field of $Ba_2YCu_3O_7$, Phys. Rev. B. 39 (1989), 2932 – 2935. https://doi.org/10.1103/PhysRevB.39.2932.
17. B. Oh, K. Char, A. D. Kent, M. Naito and M. R. Beasley, T. H. Geballe, R. H. Hammond, and A. Kapitulnik., Upper critical field, fluctuation conductivity, and dimensionality of $YBa_2Cu_3O_{7-x}$, Phys. Rev. B. 37 (1988), 7861 – 7864. http://dx.doi.org/10.1103/PhysRevB.37.7861.
18. R. V. Vovk, M. A. Obolenskii, Z. F. Nazyrov, I. L. Goulatis, A. Chroneos, and V. M. Pinto Simoes, Electro-transport and structure of 1-2-3 HTSC single crystals with different plane defects topologies, J. Mater Sci.: Mater. Electron., 23 (2012), 1255 – 1259. https://doi.org/10.1007/s10854-011-0582-8.
19. G. Lacayo, G. Kästner, R. Herrmann, Twin to tweed transition in $YBa_2Cu_3O_{7-\delta}$ by substitution of Al for Cu, Physica C. 192 (1992), 207 – 214. https://doi.org/10.1016/0921-4534(92)90762-2.
20. A. V. Bondarenko, V. A. Shklovskij, M. A. Obolenskii, R. V. Vovk, A. A. Prodan, M. Pissas, D. Niarchos, and G. Kallias, Resistivity investigations of plastic vortex creep in $YBa_2Cu_3O_{6.95}$ crystals, Phys. Rev. B. 58 (1998), 2445 – 2447. https://doi.org/10.1103/PhysRevB.58.2445.
21. P. Schleger, W. N. Hardy, B. X. Yang, Thermodynamics of oxygen in $Y_1Ba_2Cu_3O_x$ between 450°C and 650°C, Physica C. 176 (1991), 261 – 273. http://dx.doi.org/10.1016/0921-4534(91)90722-B.
22. R. V. Vovk, M. A. Obolenskii, A. A. Zavgorodniy, A. V. Bondarenko, I. L. Goulatis, A. V. Samoilov, A. Chroneos, Effect of high pressure on the fluctuation conductivity and the charge transfer of $YBa_2Cu_3O_{7-\delta}$ single crystals, J. Alloys and Compaunds. 453 (2008), 69 – 74. https://doi.org/10.1016/j.jallcom.2006.11.169.
23. M. V. Sadovskii, Pseudogap in high-temperature superconductors, Phys. Usp. 44 (2001), 515 – 539. https://doi.org/10.1070/PU2001v044n05ABEH000902.
24. R. V. Vovk, M. A. Obolenskii, A. A. Zavgorodniy, D. A. Lotnyk, K. A. Kotvitskaya, Temperature dependence of the pseudogap in aluminum and praseodymium-doped $YBa_2Cu_3O_{7-\delta}$ single

crystals, Physica B: Condensed Matter. 404 (2009), 3516 – 3518. https://doi.org/10.1016/j.physb.2009.05.047.
25. E. Babaev, H. Kleinert, Nonperturbative XY-model approach to strong coupling superconductivity in two and three dimensions, Phys. Rev. B. 59 (1999), 12083 – 12089. https://doi.org/10.1103/PhysRevB.59.12083.
26. P. G. Curran, V. V. Khotkevych, S. J. Bending, A. S. Gibbs, S. L. Lee, and A. P. Mackenzie, 2011. Vortex imaging and vortex lattice transitions in superconducting Sr_2RuO_4 single crystals, Phys. Rev. B. 84, 104507. https://doi.org/10.1103/PhysRevB.84.104507.
27. L. G. Aslamazov and A. I. Larkin, The influence of fluctuation pairing of electrons on the conductivity of normal metal, Phys. Lett., 26A (1968), 238 – 239. https://doi.org/10.1016/0375-9601(68)90623-3.
28. L. F. Chernogor, On the Nonlinearity in Nature and Science, V. N. Karazin Kharkiv National University, Kharkiv, 2008. (In Russian).
29. V. V. Yanovsky, Fractals: The Emergence of a New Paradigm in Physics, Universitates, 3 (2003), 32 – 50. (In Russian).
30. V. V. Yanovsky, Lectures on Nonlinear Phenomena. Volume 1, Institut monokristallov Publ., Kharkiv, 2006. (in Russian).
31. B. B. Mandelbrot, Les Objets Fractals: Forme, Hasard et Dimension, Flammarion, Paris 1975. (in French).
32. B. B. Mandelbrot, Fractals: Form, Chance and Dimension, W. H. Freeman and Company, San Francisco, 1977. https://doi.org/10.1002/zamm.19790590830.
33. B. B. Mandelbrot, The Fractal Geometry of Nature, CA-Freeman, San Francisco, 1982. https://doi.org/10.1119/1.13295.
34. J.-F.Gouyet, Physics and Fractal Structures, Springer-Verlag, New York, 1996.
35. T. Nakayama and K. Yakubo, Fractal Concepts in Condensed Matter Physics, Springer-Verlag, Berlin, Heidelberg, 2010.
36. R. M. Crownover, Introduction to Fractals and Chaos, Jones and Bartlett Publ., Boston, 1995.
37. F. C. Moon, Chaotic and Fractal Dynamics. An Introduction for Applied Scientists and Engineers, Wiley-VCH Verlag, Weinheim, 2004.
38. F. C. Moon, Chaotic Vibrations. An Introduction for Applied Scientists and Engineers, Wiley-Interscience, New Jersey, 2004.
39. B. B. Mandelbrot, Fractals and Chaos. The Mandelbrot Sets and Beyond, Springer-Verlag, New York, 2004. https://doi.org/10.1007/978-1-4757-4017-2.
40. H.-O. Peitgen, H. Jurgens, and D. Saupe, Chaos and Fractals. New Frontiers of Science, Second Edition, Springer-Verlag, New York, 2004.
41. O. V. Lazorenko, L. F. Chernogor, Fractal Radiophysics. 1. Theoretical Bases, Radio Phys. Radio Astron., 25 (2020), 3 – 77. (in Russian). https://doi.org/10.15407/rpra25.01.003.
42. M. A. Ivanov, V. S. Molodid, and Y. V. Skripnik, Fiz. Nizk. Temp. 30 (2004), 1086 – 1091. https://doi.org/10.1063/1.1808200.
43. A. I. Golov, I. B. Berkutov, S. Babuin, and D. J. Cousins, Characterization of fractals with an adsorbed superfluid film, Physica B: Condens. Matter 258 (2003), 329 – 333. https://doi.org/10.1016/S0921-4526(02)01984-1.
44. L. F. Chernogor, O. V. Lazorenko, A, A, Onishchenko, Fractal Analysis for Low Temperature Physics, Fiz. Nizk. Temp. 49 (2023), 459 – 465. https://doi.org/10.1063/10.0017581.
45. K. Falconer, Fractal Geometry. Mathematical Foundations and Applications, John Wiley & Sons Ltd., Chichester, 2014. https://doi.org/10.1002/0470013850.
46. J. Feder, Fractals, Springer, New York and London, 1988. https://doi.org/10.1007/978-1-4899-2124-6.
47. M. A. Haidekker, Advanced Biomedical Image Analysis, John Wiley & Sons. Inc., 2011.
48. O. V. Lazorenko, L. F. Chernogor, Fractal radiophysics. 2. Fractal and multifractal analysis, Radio Phys. Radio Astron. 28 (2023), 5 – 70 (in Ukrainian). https://doi.org/10.15407/rpra28.01.005.